The 6th International Supercritical CO_2 Power Cycles Symposium
March 27 - 29, 2018, Pittsburgh, Pennsylvania

Corrosion of Heat Exchanger Alloys in Open-Fired sCO_2 Power Cycles

Steven Kung,[†*] John Shingledecker,[†] Ian Wright,[‡] Adrian Sabau,[#] Brett Tossey,[+] and Tapasvi Lolla[†]

[†] Electric Power Research Institute, Charlotte, NC

[‡] WrightHT, Inc., Denver, CO

[#] Oak Ridge National Laboratory, Oak Ridge, TN

[+] Det Norske Veritas USA, Inc., Dublin, OH

Dr. Steven Kung is a Technical Executive in the Materials & Chemistry Department of the Electric Power Research Institute (EPRI). He leads research in areas related to corrosion and controls. Prior to joining EPRI in 2015, Dr. Kung had worked for Babcock & Wilcox Company for 25 years as well as other research laboratories in steel and glass industries. His expertise includes high-temperature and low-temperature corrosion, steam oxidation, electrochemistry, surface chemistry, diffusion coating, and water chemistry. Dr. Kung has authored more than 80 technical publications and awarded 7 U.S. patents.

*Corresponding Author: skung@epri.com

Abstract

A project was performed to develop a computational model capable of predicting the influence of oxide scales resulting from high-temperature corrosion on the service performance of metallic heat exchangers in supercritical CO_2 (sCO_2) power cycles. The model is a modification of an existing EPRI mathematical model originally developed for the prediction of oxide growth and exfoliation in boiler tubes operating in high-temperature steam. The expanded model is now capable of taking into account the thermal and mechanical parameters unique to the growth and failure of oxide scales in the heat exchangers of supercritical CO_2 power systems. To further improve the accuracy of the expanded EPRI Model, oxidation data were generated from a series of short and long-term isothermal laboratory tests in the project, in which candidate commercial alloys were subjected to a simulated sCO_2 working fluid at high temperatures and 200-bar pressure for up to 5kh. These corrosion data were incorporated into the modified model to allow it to account for the unique combination of extremely high heat-transfer conditions and complex component geometries anticipated in open-fired sCO_2 power systems. Results of the laboratory corrosion tests and application of the predictive model for the sCO_2 power cycles are presented in this paper.

Keywords: sCO_2, Oxidation, Carburization, Corrosion, Model, Heat Exchanger

Introduction

Supercritical CO_2 (sCO_2) Brayton cycles operating at temperatures greater than 600°C offer the potential to significantly improve plant efficiency for future electric power generation. However, limited data are available in the open literature on the oxidation behaviors of structural alloys exposed to sCO_2 at the high temperatures and pressures involved. The lack of relevant corrosion data has hindered the development of a computational model useful for reliable design of the small channel heat exchangers in these advanced cycles, such as gas heaters and recuperators. It is generally assumed that the oxidation kinetics and scale morphology of an alloy exposed to sCO_2 are similar to those in high-temperature high-pressure steam. However, unlike steam oxidation, the consumption of oxygen atoms from CO_2 during oxidation would lead to increased carbon activity in the working fluid and consequently carburization of the alloys, especially when the oxygen potential is low, as is the case anticipated for closed CO_2 Brayton cycles. As a result, the oxidation mechanisms operating on alloys in heat exchangers under sCO_2 may have some differences from those under high-temperature steam. The extent of any such differences must be well understood before a reliable computational model can be developed for materials selection for advanced sCO_2 power cycles.

The initial activities of this project included a comprehensive literature review of the current knowledge of materials for use in supercritical CO_2 at high temperatures. This review identified several alloys with the potential for application in the highest-temperature components in the proposed sCO_2 power cycles. These activities also included discussions with designers and technologists on the expected compositions of CO_2 present in the proposed cycles to provide a focus for the experimental work included in the project. Based on these efforts, a shortlist of seven alloys from three major alloy groups was selected for laboratory testing. In addition, analyses were made to determine the most significant types and levels of impurities likely to be present in the supercritical CO_2 working fluid so that the conditions of proposed open-fired sCO_2 power cycles could be properly simulated.

A series of short and long-term isothermal laboratory tests was conducted by exposing the selected alloys to a simulated sCO_2 working fluid containing impurities at the expected levels for natural gas combustion in open-fired sCO_2 Brayton cycles. These corrosion tests were performed at 650-750°C and 200-bar pressure for up to 5kh. The oxidation data generated were incorporated into an existing EPRI Oxide Exfoliation Model that was originally developed based on the oxidation kinetics, scale morphologies, and heat exchanger parameters associated with utility steam boilers. The modifications made allow the potential impact of oxide scale growth on the service lifetimes of compact heat exchangers using sCO_2 to be evaluated.

This work considered only the impact of oxidation and corrosion on the performance of sCO_2 power cycles. Other failure modes, such as creep, creep-fatigue, and those associated with joining and fabrication processes, etc., while also important, were considered beyond the scope of this project.

Three scenarios were considered in the application of the computational model for oxide growth in small channel heat exchangers proposed for sCO_2 recuperators: (1) change in pressure drop due to oxide thickening, (2) time to rapid oxidation due to exhaustion of the alloy chromium reservoir, and (3) time to reach a critical scale thickness for exfoliation, which leads to the need to define a threshold for blockage due to exfoliation. The modeling results indicated that reduction in flow area by simple oxide growth as well as accumulation of exfoliated scale would have the highest effect on the design of compact heat exchangers. In addition, the specific oxidation behavior of each alloy strongly influences the relationship between channel wall thickness and service lifetime. Specific predictive equations, formulated in this project are available for other researchers to use in similar component design considerations.

Experimental Procedures

Alloy selection for heat recuperators and fired heaters depends heavily on the design of the pressure boundary in sCO_2 power systems. For example, in a printed-circuit heat exchanger, the heat-transfer surfaces not only recover sensible heat but also serve as the pressure boundary. On the other hand, in fin-and-plate design, only the plate and casing are true pressure boundaries and thus much of the surface is not subject to ASME Boiler and Pressure Vessel code rules. Therefore, depending on the design and pressure requirements, a wider range of materials can be considered, including alloys that have excellent resistance to oxidation but lower strength at high temperatures. Consequently, the following criteria were primarily followed in this study to select a total of seven alloys for evaluation:

- The alloys must be commercially available so that the results are useful to compact heat-exchanger manufacturers.
- The ability of alloys must be capable of service at the intended operating temperatures.
- A small quantity of alloy samples can be procured for testing.
- Experimental results can be compared to experience gained from well-understood high-temperature steam service conditions (i.e., oxidation rates and oxide scale morphologies).
- Active interest exists in the materials on the part of heat-exchanger manufacturers.
- Alloys must be reasonably affordable in large-scale manufacturing (in terms of being both cost-competitive and cost-effective).

Based on these criteria, the following seven alloys were selected:

- Ferritic steels: Grade 91 (T91), VM12, and Crofer 22H.

- Stainless steels: TP304H and HR3C.
- Nickel-based alloys: IN617 and IN740H.

The actual compositions of these alloys were analyzed and are summarized in Table 1. Additionally, brazed and diffusion-bonded component samples of compact heat exchangers were obtained from two commercial manufacturers for inclusion in the long-term laboratory corrosion test.

Table 1 - Actual chemical compositions of the seven alloys used in this study

Element	Grade 91/T91	VM12	Crofer 22H	TP304H	HR3C	IN617	IN740H
Al	0.01	0.01	0.01	<0.01	0.01	1.13	1.33
B	0.002	0.004	<0.001	0.001	0.001	0.002	0.001
Ce	-	-	-	<0.01	<0.01	<0.01	<0.01
Ca	<0.01	<0.01	<0.01	-	-	-	-
Co	0.02	1.47	0.02	0.22	0.08	11.44	20.28
Cr	8.39	11.2	22.71	18.42	25.13	22.19	24.53
Cu	0.09	0.08	0.01	0.18	0.03	0.03	0.01
Fe	-	-	-	70.33	52.39	1.55	0.12
La	<0.01	<0.01	0.06	-	-	-	-
Mn	0.44	0.39	0.43	1.8	1.19	0.09	0.26
Mo	0.93	0.36	0.01	0.22	0.1	9.5	0.32
Nb	0.06	0.03	0.5	0.01	0.44	0.06	1.49
Ni	0.13	0.36	0.26	8.13	19.85	53.31	50.04
P	0.014	0.015	0.018	0.028	0.015	<0.002	<0.002
Si	0.24	0.41	0.29	0.48	0.4	0.08	0.15
Sn	0.01	<0.01	<0.01	<0.01	<0.01	<0.01	<0.01
Ta	<0.01	<0.01	<0.01	<0.01	<0.01	<0.01	<0.01
Ti	<0.01	<0.01	0.08	<0.01	<0.01	0.35	1.36
V	0.18	0.2	0.02	0.05	0.05	0.03	0.01
W	0.15	1.6	1.9	0.01	<0.01	0.13	<0.01
Zr	<0.01	<0.01	<0.01	<0.01	<0.01	<0.01	0.02
As	0.0038	0.0029	0.0019	0.0025	0.0021	0.0002	<0.0001
Bi	<0.00001	<0.00001	<0.00001	0.0008	0.00006	0.00007	0.00017
Pb	0.00005	<0.00001	0.00007	-	-	-	-
Sb	0.00077	0.00041	0.0001	-	-	-	-
C	0.08	0.12	0.004	0.043	0.066	0.091	0.024
S	0.001	0.001	0.002	0.002	0.001	<0.001	0.002
O	0.0032	0.0037	0.0032	0.0032	0.0016	0.0005	0.0006
N	0.0447	0.0359	0.017	0.0604	0.238	0.0065	0.004

In early commercialization of open (Allam) sCO_2 power cycles, methane firing as the heat source is likely the most economical and attractive approach. The approximate levels of impurities in the CO_2 working fluid for a prototype methane-fired sCO_2 power cycle were estimated in an associated patent [1]. To further validate the impurity concentrations, detailed thermodynamic calculations were performed for oxy-combustion of methane at 2% excess O_2 at 700°C and 200 bar using commercial software, *HSC Chemistry 8* [2]. In these calculations, both mass balance and Gibbs energy minimization were considered

simultaneously to allow redistribution of chemical species through reactions in the system to reach equilibrium. Such calculations are especially important for corrosive species of interest, which typically exist in low concentrations and thus cannot be easily estimated by means of mass balance alone. Results of the thermodynamic calculations indicated that O_2 and H_2O were the major impurities present from methane combustion in CO_2 at the turbine inlet, with the concentrations being 3.6 and 5.3 mole%, respectively. No other impurities, including sulfur-containing species would exist in meaningful quantities from methane combustion to cause corrosion concerns. The impurities of O_2 and H_2O were implemented in the laboratory corrosion testing at these calculated concentrations.

A high-temperature, high-pressure laboratory corrosion test facility was assembled to perform testing in sCO_2 at 200 bar and temperature up to 750°C. A schematic diagram of the test system is shown in Figure 1. The major system components consisted of a custom-built reaction chamber, a high-pressure pneumatic-powered gas booster pump, a water injection pump; and a high-temperature furnace. The pressure of sCO_2 was controlled by multiple stages of solenoid valves and a pressure-relief valve. The isothermal zone of the furnace in which the alloy specimens were positioned was approximately 356-mm long. This zone was calibrated to +/-5.5°C when the test temperature was controlled at 760°C.

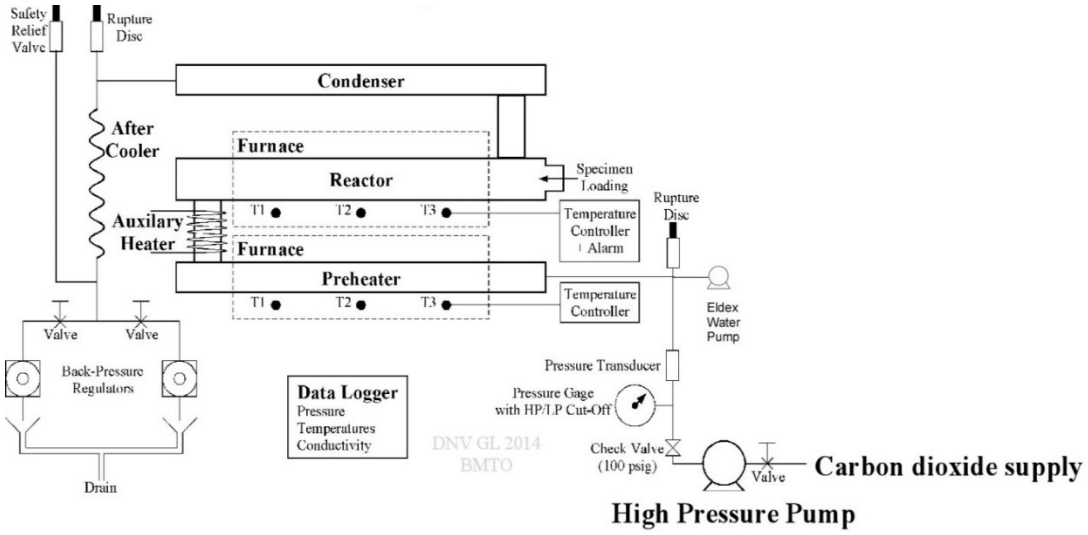

Figure 1 - Diagram of the high-temperature high-pressure corrosion test facility

The test specimens used had dimensions of approximately 2.54 x 2.54 x 0.32 cm, and all surfaces were polished to a 600-grit finish. The weight and dimensions of each specimen were measured prior to corrosion testing. In the reaction chamber, the specimens were positioned in vertical slots in a tray (made of Alloy IN625), as shown in Figure 2, so that the large surfaces were perpendicular to the gas flow direction.

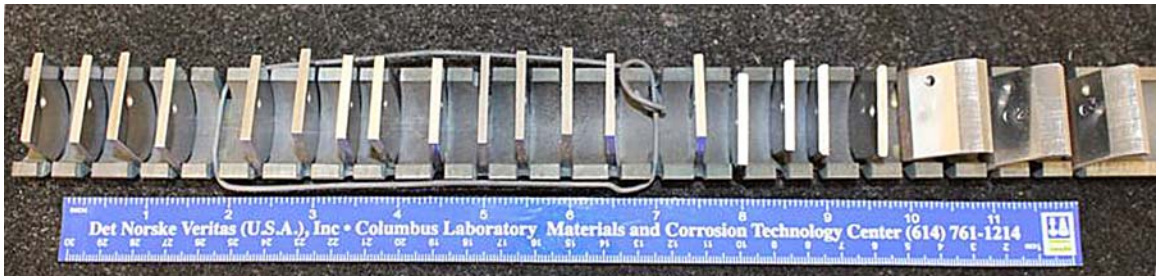

Figure 2 – Alloy specimens in tray used for high-temperature laboratory exposures.

For this study, the laboratory exposures were conducted in the temperature range of 600-750°C and at 200 bar. The ability of the test facility to achieve the desired experimental conditions and operate safely for the required test durations was validated by first running two 300-hour 'shakedown' tests at 700°C using alloys Gr 91, TP304H and IN740H. After these validation tests, a series of longer-term exposures for all seven alloys (Table 1) was performed at 650, 700, and 750°C for 1,000h each, followed by a final longer-term test up to 5,000h at 700°C in which a few additional component samples from prototype compact heat exchangers were also included.

After the exposures, the specimens were reweighed and sectioned along the centerline using a precision-cutting, diamond wafer blade operated at a low speed. One of the sectioned pieces from each specimen was mounted vertically in conductive epoxy, ground to remove approximately 3 mm of the material from the cut surface, then polished sequentially down to 0.5-µm diamond paste and finished with a 0.1-µm suspended colloidal silica. The mounted and polished cross sections were examined using an optical microscope and a scanning electron microscope (SEM) in secondary electron (SE) and backscattered electron (BSE) modes. The SEM was also equipped with energy-dispersive X-ray spectrometers (EDS) that allowed elemental spot analysis, area mapping, and line scans to be made.

Micro-hardness measurements were also performed on selected polished specimen cross-sections to infer the possibility of carburization that would have occurred during the laboratory exposures. An array of 7 x 14 micro-hardness measurements was made in the near-surface regions of the specimen cross-sections using a 100-g indenter, with indentations performed approximately 60 µm apart in both X and Y directions into the surface. The first row of measurements was taken about 60 µm from the alloy-scale interface to avoid any interference from the surface scale. These micro-hardness data were used to develop hardness maps in the surface areas of the exposed alloys.

Results and Discussion

Pertinent corrosion data available in the literature were collected and reviewed for various alloys exposed to pure and impure CO_2 at elevated temperatures under both atmospheric and high-pressure

testing conditions. Because of a lack of consistency among the test conditions employed in the various reported studies, especially in terms of test temperature and exposure time, Larson-Miller style plots were utilized in this study as a convenient and simple way to compare the literature data and assess their relative trends. The majority of the original corrosion data reported in the literature was expressed in mass gain; no loss of oxide scale was assumed from exfoliation.

sCO_2 Oxidation Data From The Literature

The literature corrosion data are compared in Figures 3-6 for four major alloy groups, where the legends indicate the sources of the data as well as the test pressures (in bar) and the CO_2 gas being 'dry' (d) or containing added water and impurities (w). For example, a legend of Gr91 (250d) indicates data for Grade 91 ferritic steel exposed to 'dry' CO_2 at 250 bar. When present, the impurities in the literature consisted of CO, H_2, H_2O, or O_2. Multiple impurities rarely were studied. The impurity levels of the 'dry' CO_2 are not stated here (but mostly are available in the data sources). Each Figure has flags to indicate the values of the Larson-Miller parameter corresponding to 10^5h at specific temperatures, intended as a means of facilitating comparison among the data sets for a given alloy, and among alloys.

The first group of alloys consists of 9-25Cr ferritic steels that are of interest for application in lower-temperature heat exchangers of sCO_2 power systems, exposed at temperatures generally dictated by Section 1 of the ASME Boiler and Pressure Vessel Code [3]. Figure 3 is a compilation of some of these data collected only for 'advanced' 9Cr steels from recent studies in the literature [4-9]; some scattering is evident. Nevertheless, a majority of the data points provides a reasonable trend line for alloys Gr/T91 and STBA26 (another advanced 9Cr ferritic steel) in sCO_2 containing oxidizing impurities. Comparison of the corrosion data with those of T91 and T92 in 17 bar steam [10] suggests lower mass gains in sCO_2 than steam, especially at lower ranges of the Larson-Miller Parameter. Nevertheless, the mass gains for sCO_2 and steam are reasonably similar at conditions where P = 21-23, representing the temperature range of 10^5h service at 550-650°C. This trend leads to an expectation that the scale morphologies formed in sCO_2 under various test conditions would be similar to those in steam.

A similar comparison for higher-Cr ferritic alloys (not shown) indicated that the mass gain in steam could be nearly two orders of magnitude lower than those in dry sCO_2. A point of considerable importance is that for this class of alloys, contributions to oxidation behavior from minor alloying elements, such as Si and S, can be significant. Therefore, knowledge of the actual compositions of the alloys studied in the literature is crucial for reliable comparison. Furthermore, any reduction in the availability of Cr in the alloy surface to participate in the scale-forming process, such as the formation of chromium carbides, could significantly alter the oxidation kinetics and thus the morphology of the scale formed.

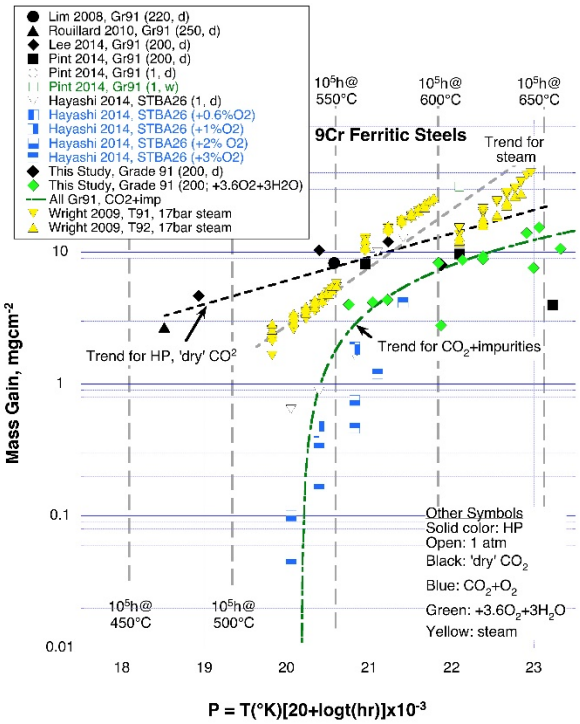

Figure 3 - Compilation of available corrosion data for ferritic steels in CO_2 from recent studies, compared to corrosion in 17 bar steam (green data points [10])

Initial observations of the scale morphologies suggest that the external oxide formed on this group of ferritic steels in sCO_2 resembles that grown in steam. Both have a double-layered microstructure with an inner layer (L1) of Fe-Cr spinel (essentially magnetite containing Cr) and an outer layer (L2) of columnar-grained magnetite. Details of the scale morphologies formed on the ferritic steels as well as other corrosion-resistant and high-strength alloys investigated in this study are presented in a separate paper [11].

Figure 4 compares the corrosion data collected for the second group of alloys consisting of several 300-series austenitic steels in 'dry' and 'impure' CO_2. The results for the conventional austenitic steels (TP304H, 321, 347) in Figure 4(a) show considerable scattering, with the dashed line indicating a possible upper bound in 'dry' sCO_2. The influence of water vapor impurities on TP321 appears to be inconclusive, but shot peening is beneficial for this alloy. Data for the advanced austenitic steels (TP347HFG and TP310/HR3C) in Figure 4(b) are relatively sparse in CO_2. Nevertheless, the upper bound line in 'dry' sCO_2 for these alloys suggests a considerable reduction in mass gain compared to the 'standard' austenitic steels. For TP310, there appears to be an accelerating effect on mass gain in CO_2 containing 300 ppm (by weight) water vapor [12].

The behaviors of austenitic steels when exposed to CO_2 or steam appear to vary with alloy. For example, the oxidation rates of TP310 in dry sCO_2 and high-pressure steam (not shown) are very similar,

while substantially higher mass gains were observed for TP347HFG in steam than dry sCO_2 (note that, however, there are relatively few data available for 'dry' sCO_2).

The third group of materials consists of different Ni-based alloys, with select corrosion data [6,13-18] compared in Figure 5. There were too few data points for sCO_2 containing controlled impurities to provide definite indications of any effect of impurity, for instance, water vapor, on this group. The upper bound for all these data points occurs at very similar mass gains to that for TP310, though some alloys (notably IN625 and IN740) exhibited significantly lower mass gains. The corrosion data for alloy IN740H [6,16,18] are plotted separately in Figure 5(b), and an extrapolation to 10^5h at 700°C is suggested by the dashed line. The data generated from the current study for IN740H exposed to impure sCO_2 containing 3.6 vol% O_2 plus 5.3 vol% H_2O imply a possible sharp reduction in the corrosion rate when oxidizing impurities are present.

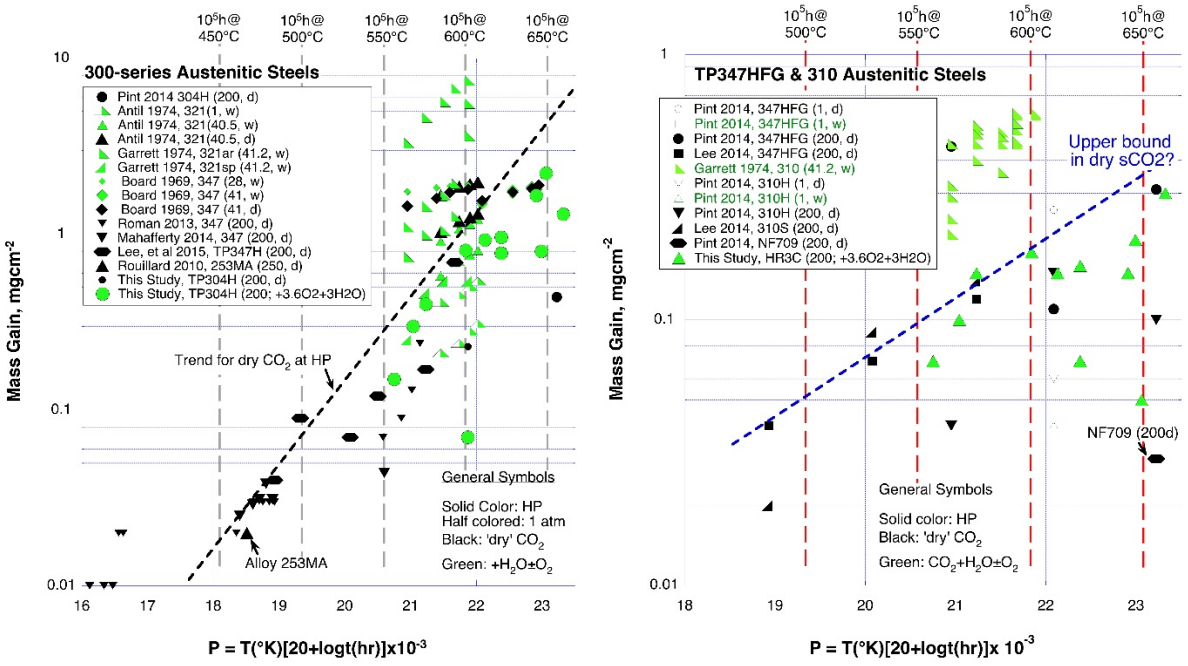

(a) **(b)**

Figure 4 - Compilation of available corrosion data for austenitic steels in CO_2: (a) conventional austenitic steels; and (b) advanced austenitic steels

Due to the abundance of corrosion data available in the literature for this group of alloys tested in steam [10], a similar Larson-Miller plot was generated in this study (not shown), which exhibited a consistent trend in mass gain to a considerably higher value of the Larson-Miller parameter with time and temperature. This consistency suggests that no change would occur in the corrosion mechanism and thus scale morphology in steam over a wide range of test conditions employed. Because a good fit was observed for the suggested upper-bound trend lines from both oxidation-resistant austenitic steels

(Figure 4b) and wrought Ni-based alloys (Figure 5b), it is expected that the corrosion behaviors of these alloys would be similar in both dry sCO_2 and steam. Consequently, these alloy classes are also expected to produce similar scale morphologies in both environments

The fourth group of materials for which data were available consists of alloys with the ability to form a protective *alpha* alumina (α-Al_2O_3) scale at relatively high temperatures (e.g., ≥900°C). At lower temperatures, however, the more rapidly-growing but less protective *gamma*-Al_2O_3 is usually formed, resulting in mass gains similar to those of chromia-forming alloys under the same test conditions. Compilation of the available corrosion data for several of such alumina-forming Ni-base alloys in a Larson-Miller plot (not shown) did reveal such similarity in mass gain, although some specially alloyed and processed alumina-forming alloys exhibited mass gains considerably below the suggested upper bound for chromia-forming alloys.

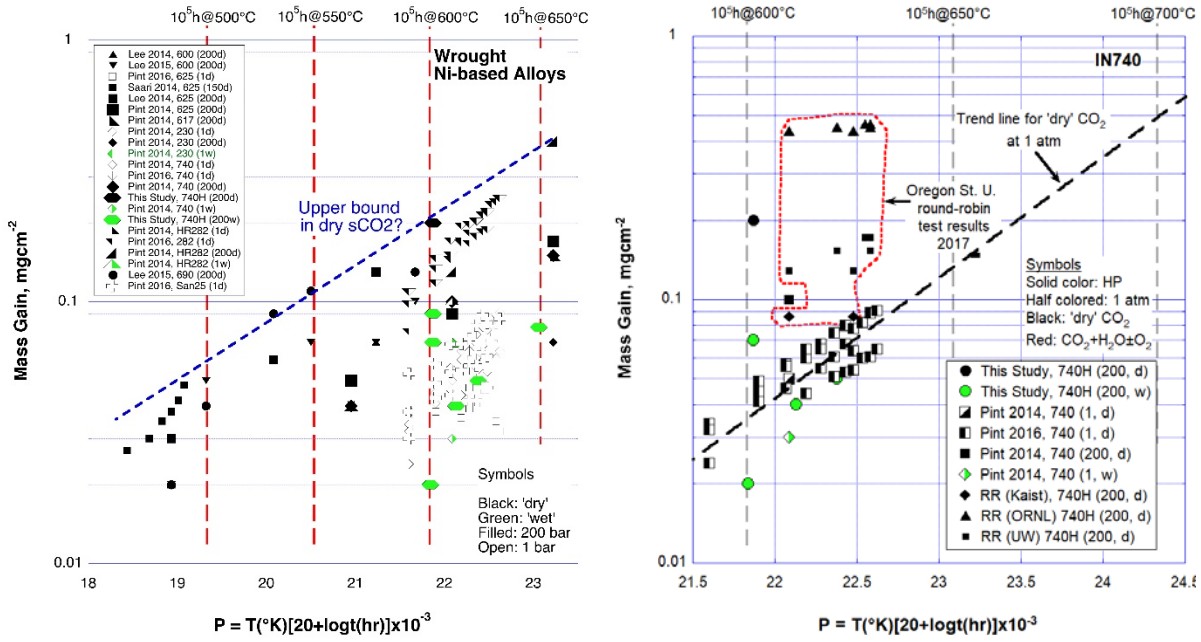

(a) **(b)**

Figure 5 - Compilation of available corrosion data for wrought Ni-based alloys in CO_2: (a) all alloys; and (b) data for IN740 with extrapolation to 700°C ('RR' signifies results from Oregon State University sCO_2 Round Robin group, J. Tucker, Aug 2017)

<u>sCO_2 Oxidation Data From This Work</u>

The EPRI Oxide Scale Exfoliation Model requires algorithms to describe the rate of oxide scale thickening in terms of time and local metal temperature. As a result of practical difficulties, acceptable algorithms were developed from the exposures of this study only for Grade 91 and TP304H at 650-750°C

in CO_2-3.6 vol% O_2-5.3 vol% H_2O at 200 bar. These alloys exhibited consistent scale morphologies that permitted extrapolation to a lower temperature range of 550-600°C at which they are likely to be employed. Ferritic alloys VM12 and Crofer 22H exhibited oxidation kinetics that were essentially intermediate between Grade 91 and TP304H, but the trend with temperature was inconsistent, possibly due to a transition in scale morphologies with temperature (increasing Cr diffusion rates). For the alloys that formed protective scales, such as IN740H, it proved impossible to generate sufficiently precise details of scale thicknesses and morphologies, even when using SEM at very high magnifications. As a result, thickness-based kinetics data from exposure of IN740 to high-pressure steam at 650-800°C were utilized for the model simulations. The Arrhenius constants on which the algorithms for oxidation in sCO_2 used in the modification of the EPRI Model are based are shown in Table 2 (based on mass gain) and Table 3 (based on oxide thickness).

Table 2 - Mass gain-based Arrhenius constants for oxidation in sCO_2

Alloy	Environment	T Range (°C)	A_{Am} (g^2/cm^4s)	Q_m (kJ/mole)	R^2
Grade 91	CO_2 at 200 bar	650-750	1.12×10^{8}	-372	0.92
TP304H	CO_2 at 200 bar	650-750	1.87×10^{-6}	-136	1.00
IN740	Steam at 17 bar	600-800	3.2×10^{-3}	-229	0.98
HR3C	Steam at 17 bar	650-800	6.0×10^{3}	-338	0.87

Table 3 - Thickness- based Arrhenius constants for oxidation in sCO_2

Alloy	Environment	T Range (°C)	A_{At} ($\mu m^2/h$)	Q_t (kJ/mole)	R^2
Grade 91	CO_2 at 200 bar	650-750	2.8×10^{19}	-376	0.88
TP304H	CO_2 at 200 bar	650-750	1.1×10^{6}	-151	0.99
IN740	Steam at 17 bar	650-800	1.4×10^{5}	-166	0.97

Plots of total scale thickness as a function of time and temperature, based on the recommended oxidation algorithms, are shown in Figure 6 for the isothermal oxidation of alloys Grade 91, TP304H, and IN740H. Figure 6a illustrates a large increase in rate of scale growth for Grade 91 at 650°C compared to 600°C, and suggests an oxidation-based temperature limit for this alloy commensurate with recently-recommended temperature limits for steam boilers of 580-600°C [23]. Similarly, the rate of scale growth on TP304H (Figure 6b) appears to accelerate significantly above 650°C, suggesting that it be restricted to use at or below this temperature. While the rate of scale growth on IN740H (shown in Figure 6c) also appears to begin to accelerate above 700°C, the actual thickness values are sufficiently low that application of this alloy (in terms of oxidation rate) up to 750°C appears to be justified.

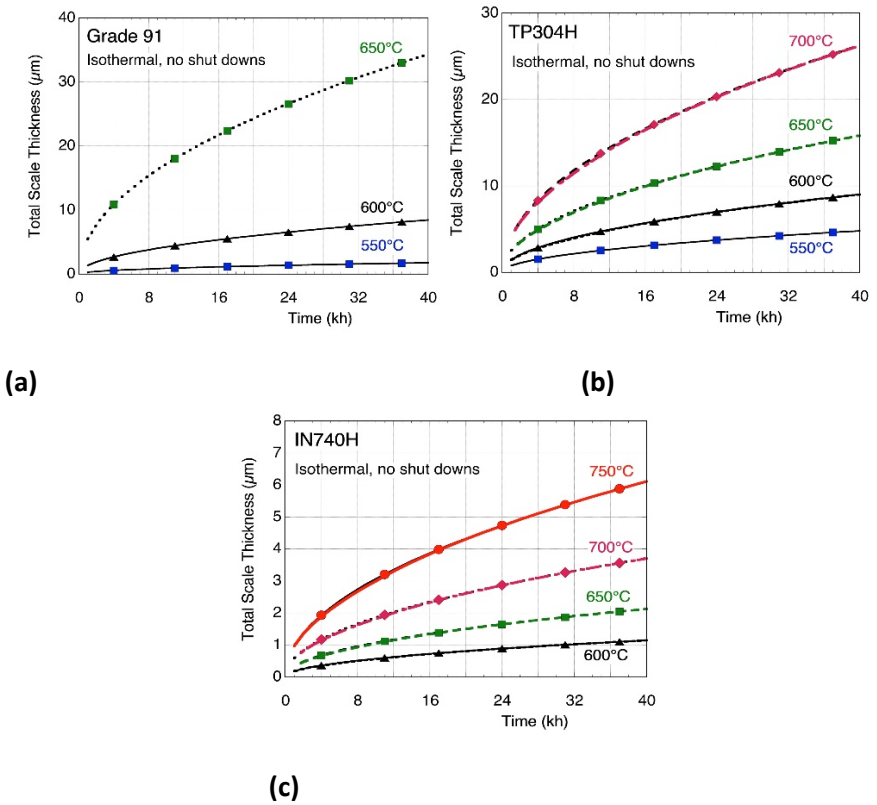

Figure 6 - Thickness-based oxidation kinetics from algorithms derived for use in the EPRI Oxide Exfoliation Model. Note that the data for alloys (a) Grade 91 and (b) TP304H are from exposures in sCO_2-3.6 vol% O_2-5.3 vol% H_2O at 200 bar and 650-750°C. Those for (c) IN740H were taken from exposures in 17 bar steam at 650-800°C.

Microhardness Measurements

As mentioned previously, micro-hardness measurements were performed in this study to estimate the extent of carburization of the exposed specimen surfaces during the sCO_2 exposures. A micro-hardness map and the corresponding profile for ferritic Grade 91 after exposure to sCO_2 containing 3.6 vol.% O_2 and 5.3 vol.% H_2O at 700°C and 200 bar for 1,000h are shown in Figure 7. The wide distribution of areas with relatively elevated hardness (shown in red, pink, and yellow) in Figure 6a suggests that possibly some carburization occurred near the surface. The hardness profile in Figure 6b indicates an increase of surface hardness after 1,000h to a depth of 350+ µm, which is significantly beyond the depth measured after the 300h exposure (not shown). Such an increase in hardness profile with time indicates that the surface harness was not caused by cold work from initial specimen preparation, since increasing exposure time from 300 to 1,000h at 700°C would have significantly reduced any such cold work effects.

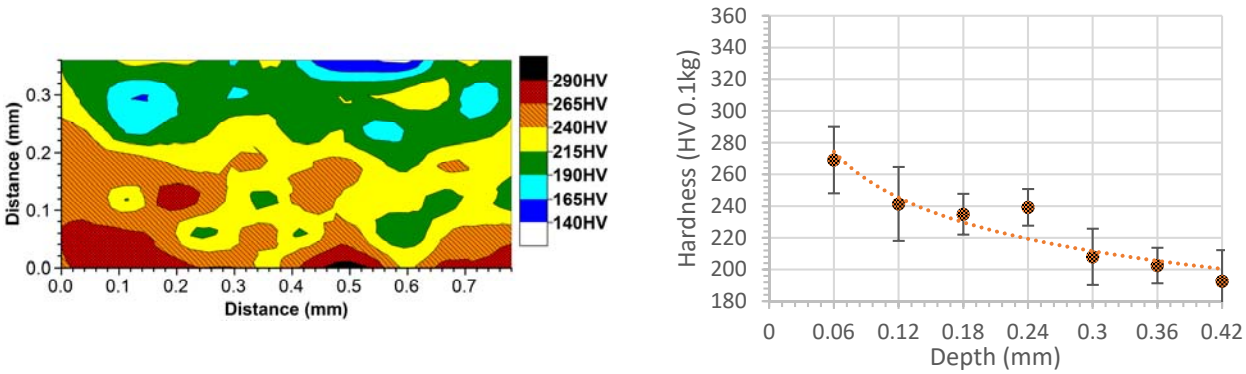

Figure 7 - Hardness distribution and profile near the surface of ferritic Grade 91 after exposure to sCO_2 containing 3.6 vol.% O_2 and 5.3 vol.% H_2O at 700°C and 200 bar for 1,000h, where alloy-oxide interface is at Distance 0.0

An increase in surface hardness was also observed for ferritic VM12 after exposure to sCO_2 containing 3.6 mole% O_2 and 5.3 mole% H_2O at 700°C and 200 bar for 1000h, as shown in Figure 8. The depth of carburization zone in VM12 appears to exceed 300 µm after 1000 hours. Based on the results of both Grade 91 and VM12, it is reasonable to assume that ferritic alloys with a relatively low Cr contents (9-12 wt.%) would be susceptible to carburization attack in sCO_2, even for a working fluid containing large amounts of O_2 and H_2O as oxidizing impurity.

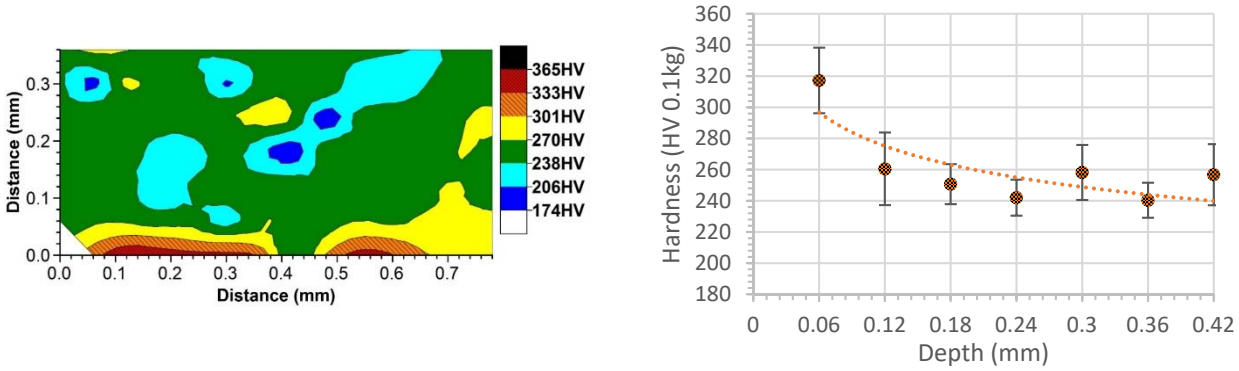

Figure 8 - Hardness distribution and profile near the surface of ferritic VM12 after exposure to sCO_2 containing 3.6 vol.% O_2 and 5.3 vol.% H_2O at 700°C and 200 bar for 1,000h, where alloy-oxide interface is at Distance 0.0

A lack of obvious hardening suggested that little carburization occurred in Crofer 22H after exposure to the impure sCO_2 conditions at 200 bar and 700°C for 1000h. Obviously, the higher Cr content (approximately 22 wt.%) in Crofer 22H would have led to the formation of a relatively more corrosion-resistant scale at 700°C and thus provided better carburization resistance than for lower grade VM12 and Grade 91. Evidence of a hardness increase was found at the surface of TP304H after exposure to impure

sCO_2 containing 3.6 vol.% O_2 and 5.3 vol.% H_2O at 200 bar and 700°C for 300h. However, the surface hardness profile became uniform after testing in the same conditions for 1000h, suggesting that the scale formed on TP304H became increasingly more corrosion-resistant with time.

A hardness map and corresponding profile for HR3C after exposure to sCO_2 containing 3.6 vol.% O_2 and 5.3 vol.% H_2O at 200 bar and 700°C for 1000h are shown in Figure 9. The hardness profile is presented as a box-and-whisker plot to highlight the statistics of the hardness readings. Typically, a high total concentration of Cr and Ni is beneficial for alloys to resist carburization. Surprisingly, compared to Crofer 22H and TP304H, carburization on HR3C appears to be more severe, with increased hardness measured up to a depth of approximately 0.15 mm (150 µm) from the alloy surface. It is likely that the high Cr content (25 wt.%) in this alloy promoted carbon ingress by forming chromium carbide (likely $Cr_{23}C_6$) during the 1000h laboratory exposure at 700°C. Apparently, the amount of Ni present in HR3C at approximately 20% was insufficient to suppress carburization.

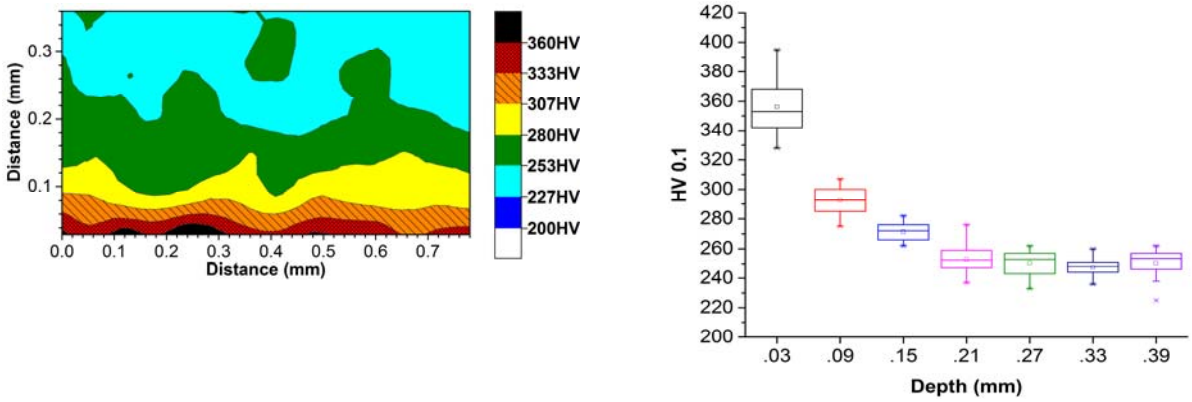

Figure 9 - Hardness distribution and profile near the surface of HR3C after exposure to sCO_2 containing 3.6 vol.% O_2 and 5.3 vol.% H_2O at 200 bar and 700°C for 1,000h, where alloy-oxide interface is at Distance 0.0

The results of micro-hardness measurements for IN617 and IN740H did not reveal any evidence of carburization. Obviously, these alloys contain sufficient Cr and are Ni-based. Therefore, they possess inherently strong carburization resistance. Judging by the satisfactory resistance of Crofer 22H (relatively high Cr, no Ni, and very low C) and poor resistance of HR3C (relatively high Cr, insufficient Ni, but high C) to carburization, it appears that the selection of a high-Cr nickel-based alloy (likely containing more than 22% Cr) would be required for application in the high-temperature sections of heat exchangers in sCO_2 Brayton power cycles. As demonstrated by the corrosion rates shown in Figure 5, nickel-based alloys containing high Cr and Ni also offer superior oxidation resistance.

Modification of the EPRI Oxide Exfoliation Model

The EPRI Oxide Exfoliation Model [19-21] was modified to include relevant input parameters common to the design of heat exchangers intended for use in sCO_2 Brayton power cycles. These parameters consisted of additional materials properties, physical configurations of flow channels and associated heat transfer and fluid flow criteria, and updated oxidation kinetics (based on data generated from this work and select literature studies). Furthermore, one of the key conclusions derived from this project, as discussed above, was that the oxide kinetics and scale morphologies formed on different classes of alloys after exposure to sCO_2 and high-pressure steam could be considered, to a first approximation, similar. Therefore, the extensive available data on oxidation behavior in steam was considered a viable starting point for the model modification.

Similar to steam oxidation, oxide scales grown on the surfaces of sCO_2 heat-exchanger flow channels were considered to be nearly stress-free at high temperatures. The relevant sources of stress were those generated during excursions to low temperatures from differences in coefficients of thermal expansion between the alloy substrate and various layers of oxide scales, stresses from mechanical constrains due to geometric features, and those from changes in system pressure. Once the scales are sufficiently thick that the stress developed exceeds some critical value (e.g., during a rapid shut-down event), failure of the scale by one or more of several possible modes [22] would be expected, and exfoliation becomes likely. As an example of model output, some initial results predicted by the modified EPRI Oxide Exfoliation Model for the total mass of exfoliated scale in circular-section flow channels of TP347H are presented in Figure 10.

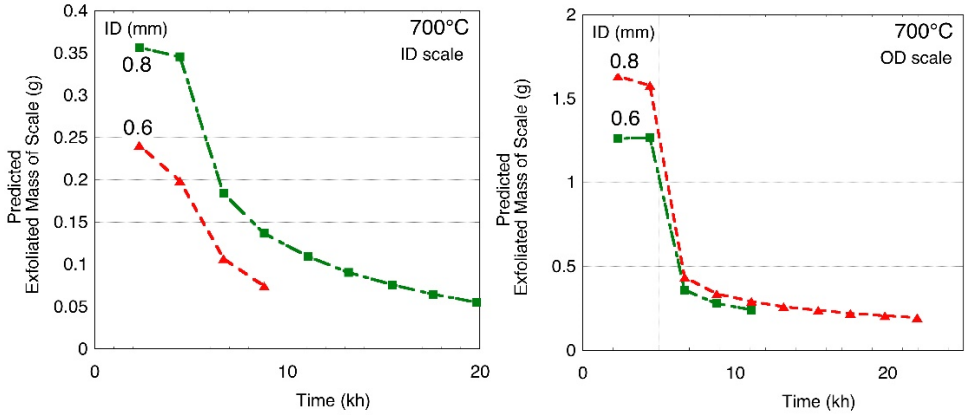

(a) (b)

Figure 10 - Predicted mass loss with time of magnetite exfoliated for a circular section flow channel of TP347H (2mm-thick walls, 0.5m total length): (a) scale grown on inner surface and (b) scale grown on outer surface.

In these initial simulations the circular channels were assumed to have a 0.5m-long flow path and 0.2mm wall thickness but differ in inner diameter (ID). Both channels were operated with regular shut-down events occurring at 3-month (2.2kh) intervals, at which times the exfoliated scale was removed from the channels. Only an outer (magnetite) layer was considered to exfoliate from the scale formed on TP347H (as occurs in steam). The results indicate that a larger amount of scale would exfoliate as the tube diameter increased. In addition, a significantly larger amount of oxide (approximately 5x) would exfoliate from the outside (convex) surfaces than the inside (concave) surfaces at any given time. The main reason for this difference is that, during cool down a tensile stress would be imposed of the scale formed on the (larger) outer surface by the retreating alloy, whereas the scale on the inner surface would experience a net compressive stress.

In the absence of any practical field experience for alloys that form more protective scales than TP347H (such as IN740H), assumptions were required about how the exfoliation process should be treated by the model. The approach adopted was to assume that a single-layered scale of uniform thickness was formed; accordingly, all the oxide grown at a given temperature should attain a thickness commensurate with the critical strain for failure at approximately the same time, and would be lost at the first corresponding exfoliation event. Subsequently, no further exfoliation would be expected until sufficient time had elapsed that the scale has again attained the critical thickness/strain. If as assumed the full scale thickness were removed, the rate of re-oxidation of the exposed alloy surface would be the same as that at the original exposure. In practice, since the scale likely may not be uniform in thickness, a mass loss vs. time curve probably would consist of spikes of major (but possibly not total) loss, interspersed with periods of no loss where the scale had not reached the critical thickness. This proposed exfoliation mechanism also was incorporated into the model.

Application of the EPRI Oxide Exfoliation Model to sCO_2 Recuperator Conditions

Since the formation of surface oxide scales is inevitable for alloys exposed to high-temperature environments, it is important to recognize how they can affect operation and performance of sCO_2 compact heat exchangers. Three scenarios were considered whereby the growth of an adherent, protective oxide scale on the walls of a heat exchanger can affect its service life:

1. Reduction in available flow area (RFA_{ox}) as the oxide scale on the surfaces of the flow passages thickens with time.
2. Depletion of Cr at the tube wall surface (due to the formation of a Cr-rich protective scale) to a level where faster-growing, less protective oxide could develop; and
3. Exfoliation of scale when some critical level of accumulated strain is reached, leading to release of flakes of oxide into the flow stream and potential blockage of the flow passages. This scenario involves two connected considerations: (a) the time to attain the critical oxide strain at which

scale failure or exfoliation becomes possible and (b) the acceptable threshold for blockage (% open area).

Relative to Scenario 1, the design of small flow channels and high flow rates in sCO_2 power systems requires the absence of any significant increase in pressure drop to maintain intended efficiency. Inevitably, the rate of thickening of oxide scale and its influence on pressure drop become an important consideration. Figure 11 illustrates the predicted relationship between an increase in pressure drop and reduction in flow area (%RFA).

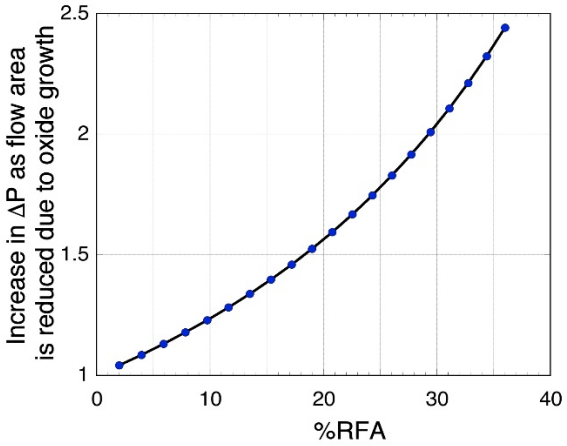

Figure 11 - Relationship between reduction in flow area (%RFA) and increase in pressure drop for laminar flow through a circular channel.

Based on the use of algorithms for oxidation kinetics (as shown in Figure 6) in the EPRI Oxide Exfoliation Model, the times to achieve 1%, 2%, and 5% RFA for 0.3mm-diameter channels of alloys Grade 91, TP304H, and IN740H are compared in Table 4 over the temperature range of 550 to 750°C; also included are the times for 0.6mm and 0.9mm-diameter channels to achieve 5% RFA. Note that these values required some extrapolation of the oxidation algorithms since actual oxidation kinetics were measured only for 650-750°C. For example, the time to reach a scale thickness of 7.6 µm/5%RFA in a 0.6mm-diameter channel would be attained in 32,400h (3.7yr) for Grade 91 at 600°C, 9,216h (1.1yr) for TP304H at 650°C, and 61,711h (7.1yr) for IN740H at 750°C (168,236h/19.3yr at 700°C). Some other examples are shown in Table 4, which indicate that the use of 0.3mm-diameter channels would lead to unacceptably short service lifetimes, even for IN740H at 700°C. Limiting RFA to 1% would further reduce the lifetime of 6mm-diater channels of IN740H to 6,641h at 700°C, and 9mm-diameter channels to 14,678h at 700°C.

Table 4 - Predicted times to reach specified values of RFA_{ox} in sCO_2-3.6 vol% O_2-5.3 vol% H_2O at 200 bar

Alloy	T°C	Time (h) to Reach Stated %RFA				
		0.3 mm Channel			0.6mm	0.9mm
	RFA_{ox}:	*1%*	*2%*	*5%*	*5%*	*5%*
Grade 91	**600**	320	1,280	8,100	32,400	72,700
VM12	**600**	30	140	870	3,470	7,800
TP304H	**650**	90	364	2,304	9,216	20,699
IN740H	**700**	1,638	6,641	42,059	168,236	377,867

In consideration of Scenario 2, the ability of an alloy to form a protective outer oxide scale (usually chromia or a Cr-rich spinel) requires the presence of a minimum (critical) level of Cr (C_B) at the alloy-environment interface. Since growth of the desired oxide consumes Cr, it is important that the level of Cr at the alloy surface is maintained above C_B to ensure that predictable, protective oxidation behavior continues. Ideally, during the course of exposure, the gradient in Cr concentration that develops from the alloy-oxide interface inward will remain small so that essentially all of the original Cr content of the alloy (C_0) in excess of the value of C_B will be available to support maintenance of the protective scale. This is generally true for ferritic alloys at higher temperatures, but for austenitic Fe-Ni-Cr and Ni-base alloys at temperatures in the range of interest, it is more usual for a noticeable Cr gradient to develop, so that the available 'reservoir' of Cr in the alloy becomes less than (C_0 - C_B).

Results of calculations of the times to reach C_B for alloys TP347H, HR3C, and IN740H with wall thicknesses of 0.2 mm exposed in CO_2-3.6 vol% O_2-5.3 vol% H_2O over the temperature range 550-750°C are summarized in Table 5. These data indicate that, based on assumptions made, the lifetimes for HR3C and IN740 at 750°C would exceed 10 yr. In contrast, TP304H would reach the (assumed) minimum level of Cr (C_B) after only 2.2 yr at 650°C. Further results for wall thicknesses of 0.3, 0.5, and 1.2 mm shown in Table 5 suggest that Scenario 2 would be life-limiting only for TP304H.

Table 5 - Times to reach critical Cr levels for onset of rapid oxide growth (end of service life) in CO_2-3.6 vol% O_2-5.3 vol% H_2O for different channel wall thicknesses

Alloy	C_b (wt% Cr)*	Temp. (°C)	Lifetime (kh)			
		Wall Thickness (mm):	*0.2*	*0.3*	*0.5*	*1.2*
TP304H	**12**	**650**	19	43	120	692
HR3C	**12**	**700**	739	1,663	4,619	26,605
IN740H	**15**	**750**	1,070	2,407	6,686	38,509

•based on experimental results for model binary alloys

In Scenario 3, the time to failure for scale exfoliation leading to oxide accumulation in the channels was calculated using the modified EPRI Oxide Exfoliation Model. Assumptions made in the calculations included a channel length of either 0.5 or 1m, with the heat exchanger being operated for three-month intervals between shutdown events and the exfoliated scale cleared out at each shutdown. Based on experiences in steam boilers, the accumulated oxide was assumed to have a porosity of approximately 25%, and the length of the accumulation debris would be 10x the channel diameter. Accumulation is assumed at locations immediately upstream of a major change in the flow passage, such as a tight bend.

Results for the 0.5 and 1.0m-long channels constructed of TP304H and IN740H with diameters 0.3 and 0.6mm are compared in Table 6. The results are expressed in time (kh) to attain a blockage value of 0.05 (RFA_B = 5%) by exfoliated scale, where the inlet and outlet temperatures are (a) 550 and 700°C for TP304H, and (b) 600 and 750°C for IN740H. The predicted blockage fraction for a 1m-long, 0.3mm-diameter TP304H channel attained a value of 0.05 (RFA_B = 5%) after 30.8kh under the conditions of 550°C inlet and 700°C outlet, compared to only 12.2kh for 600°C inlet and 750°C outlet. Similarly, sufficient exfoliation for an IN740H channel to lead to blockage equivalent to 5% RFA in a 1m-long, 3mm-diameter channel was predicted after 18.7kh, and for a 0.5m-long channel after 22.4kh, both operated at 600°C inlet and 750°C outlet temperatures.

Table 6 - Times to reach specified values of RFA_B = 5% in sCO_2-3.6 vol% O_2-5.3 vol% H_2O.

Alloy	**Temp. (°C)**	**Lifetime (kh)**			
Channel Length (m):		***0.5***		***1.0***	
Channel diameter (mm):		***0.3***	***0.6***	***0.3***	***0.6***
TP304H	***550 in-700 out***	33.9	>>40	30.8	>40
	600 in-750 out	13.2	17.5	12.2	15.6
IN740H	***600 in-750 out***	22.4	>40	18.7	28.6

Overall Implications of Oxide Growth on Service Lifetime of sCO_2 Recuperators

Because of the high temperatures at which it is planned to operate sCO_2 heat exchangers, the rate at which oxide scales grow and thicken on alloys in contact with the gas is an important consideration. Scenarios 1 and 3 discussed above are explicitly associated with oxide growth (and exfoliation), and are closely connected. While growth of protective oxide scales inevitably contributes to *progressive* reduction in flow area, flow blockage resulting from exfoliation usually is a *singular* occurrence that happens at specific intervals (associated with thermal shocks, such as heat exchanger shut-down events). A consideration of considerable importance is whether unacceptable reduction in flow area from simple (continuous) oxide growth will occur before exfoliation becomes likely. Upon restarting the heat

exchanger after the exfoliant contributing to blockage has been removed, the value of reduction in flow area associated with the affected length of channel will be reset, and the effective value of the area reduction will then be determined by the thickest adherent scale remaining in that channel.

Scenario 2 where consumption of the reservoir of Cr in the channel wall by continued growth of protective scale reduces the Cr level at the alloy-oxide interface to a value where the protective layer no longer can be supported, leading to accelerated rates of scale growth, appears to be life-limiting only for alloy TP304H (for the conditions of temperature and wall thickness considered). Obvious remedies would be to reduce the temperature and/or increase the thickness of the channel wall, or to use a more oxidation-resistant alloy. For IN740H (and presumably other corrosion-resistance alloys with similar oxidation behavior), this scenario appears to lead to lifetimes somewhat longer than those directly causing reduction in flow area (for the conditions considered).

Conclusions

Research was conducted to enable computational prediction of the effects of oxide growth on structural alloys operating under the high-temperature conditions of sCO_2 heat exchangers on the performance of those systems. This research was accomplished through modification of an existing EPRI Oxide Exfoliation Model for scale growth and exfoliation by incorporating additional data to describe both oxidation behavior in sCO_2 and specifics of the design and operation of the small channel heat exchangers under consideration. Oxidation data were generated for candidate alloys in a series of isothermal laboratory tests at 650-750^oC for 300-5,000h using sCO_2 containing 3.6 vol.% O_2 and 5.3 vol.% H_2O at 200 bar. Overall, the project was successful in producing a modified EPRI Model that can be used to identify the behaviors of key candidate alloys for use in sCO_2 Brayton power cycles.

The levels of impurities in the CO_2 implemented for the laboratory tests were determined by thermodynamic and mass-balance calculations. Oxidation rates were measured for seven commercial alloys, including high-strength ferritic steels, standard and advanced austenitic steels, and Ni-based alloys. In addition, the corrosion data available for various alloys in the literature were reviewed and analyzed. Based on the compilation and comparison of all available data, it appears that rates of oxide scale growth on alloys in sCO_2 with and without impurities were similar to those under high-temperature steam, and the scale morphologies formed in both environments also were similar. However, some potential influences of carbon through carburization on the corrosion behaviors of less corrosion-resistant alloys, including ferritic Grade 91 and VM12 as well as austenitic steels, were identified by means of micro-hardness measurements. No carburization was evident in the Ni-based alloys IN617 and IN740H.

Using the EPRI Oxide Exfoliation Model, different scenarios of failure mechanisms were considered in the performance of small-channel heat exchangers: (1) increase in pressure drop due to

continuous oxide thickening, (2) time to loss of protective oxidation behavior due to exhaustion of the chromium reservoir in the alloy, and (3) time to reach a critical thickness for oxide exfoliation and the relationship between the resulting reduction in flow area from exfoliation and the accepted blockage threshold. The modeling results indicated that reduction in flow area by oxide growth, as well as channel blockage by accumulation of exfoliated scale, pose major questions for the design of small-channel heat exchangers. In particular, the specific oxidation behavior of each alloy strongly influences the relationship of channel wall thickness to service lifetime. The base equations formulated from this study are available for use by researchers in generic design of sCO_2 heat exchangers.

Acknowledgements

The authors would like to acknowledge the funding support of the U.S. Department of Energy under Contract No. DE-FE0024120 (Project Manager: Vito Cedro III).

References

1. System and Method for High-Efficiency Power Generation Using a Carbon Dioxide Circulating Working Fluid, US Patent 2011/0179799 A1, July 28, 2011.
2. HSC Chemistry for Windows, Ver. 8, Outokumpu, Finland.
3. ASME Boiler and Pressure Vessel Code, Section I: *Rules for Construction of Power Boilers*, ASME, Three Park Avenue, New York, New York, (2015).
4. A.M. Pritchard and A.E. Truswell, "Mechanistic experiments on the oxidation of 9% Cr steels in CO_2 at 550°C," Paper No. 19 in *Proc. B.N.E.S. Intl. Conf. on Corrosion of Steels in CO_2* (1974).
5. J.C.P. 11, S.K. Lister, P.J. Nolan and J.T. Crook, "Some factors in the oxidation of austenitic stainless steels," Paper No. 23 in *Proc. B.N.E.S. Intl. Conf. on Corrosion of Steels in CO_2* (1974).
6. B.A. Pint and J.R. Keiser, "The effect of temperature on the sCO_2 compatibility of conventional structural alloys," Paper no. 61 presented at the *4th International Symposium - Supercritical CO_2 Power Cycles*, September 9-10, 2014, Pittsburgh, Pennsylvania.

7. J. Board and R. Winterborne, "Oxidation of Austenitic Stainless Steel Boiler Tubing in Carbon Dioxide," *British Corrosion Journal* 4 (2), 86-93 (1969).
8. K. Kaya, S. Hayashi, and S. Ukai, "High-temperature oxidation behavior of Fe-9Cr steel in CO_2-O_2 gas mixture," *ISIJ International*, 54 (6), 1379-1385 (2014).
9. G.B. Gibbs, R.E. Pendlebury and M.R. Wootton, "Protective and breakaway corrosion of mild steel in CO_2," Paper No. 6 in *Proc. B.N.E.S. Intl. Conf. on Corrosion of Steels in CO_2* (1974).
10. I.G. Wright, DOE FWP No. FEAA061: Oxidation of Candidate Alloys in Steam at 17 bar: Final Report on Phase 1 efforts in support of the US Consortium Program on Boiler Materials for Ultra-Supercritical Coal Power Plants, ORNL/TM-2009/232 (Nov. 2009).
11. T. Lolla, J. Shingledecker, S. Kung, M. Gagliano, I. Wright and A. Sabau, Characterization of Oxide Scale Structures on Alloys exposed to Open-Fired sCO_2 Power Cycles, The 6th International Supercritical CO_2 Power Cycles Symposium, Paper #158, Pittsburgh, PA (2018).
12. J.C.P. 11, S.K. Lister, P.J. Nolan and J.T. Crook, "Some factors in the oxidation of austenitic stainless steels," Paper No. 23 in *Proc. B.N.E.S. Intl. Conf. on Corrosion of Steels in CO_2* (1974).
13. H. Saari, C. Parks, R. Petruskeno, B. Maybee, and K. Zanganeh, "Corrosion testing of high-temperature materials in supercritical CO_2," Paper no. 32 presented at the *4th International Symposium - Supercritical CO_2 Power Cycles*, September 9-10, 2014, Pittsburgh, Pennsylvania.
14. H.J. Lee, H. Kim, and C. Jang, "Compatibility of candidate structural materials in high-temperature S-CO_2 environment," Paper no. 32 presented at the *4th International Symposium - Supercritical CO_2 Power Cycles*, September 9-10, 2014, Pittsburgh, Pennsylvania.
15. H.J. Lee, H. Kim, S.H. Kim, and C. Jang, "Comparison of the corrosion behaviors of Fe-base and Ni-base austenitic alloys in high-temperature S-CO_2 environment," Section 3, Session 1A-Supercritical CO_2 Oxidation/Corrosion, Proc. EPRI International Conference on Corrosion in Power Plants (San Diego, Oct 13-15, 2015), EPRI Report No. 3002006972, Nov. 2015.
16. J.P. Shingledecker, *Predicting the Oxidation/Corrosion Performance of Structural Alloys in Supercritical CO_2,* Research Performance Progress Report on Contract DE-FE0024120, Jan 30, 2015.
17. B.A. Pint, R.G. Brese, and J.R. Keiser, "Effect of pressure and thermal cycling on compatibility in CO_2 for concentrated solar power applications," paper No. GT2017-65066, Proc. ASME Turbo Expo 2017, Charlotte, North Carolina (2017).
18. A.S. Sabau and I.G. Wright, "Influence of oxide growth and metal creep on strain development in the steam-side oxide in boiler tubes," *Oxidation of Metals*, 73, 467-492 (2010).
19. A.S. Sabau, I.G. Wright, and J.P. Shingledecker, "Oxide scale exfoliation and regrowth in TP347H superheater tubes," *Materials and Corrosion*, 63 (10), 896-908 (2012).
20. J.P. Shingledecker, A.T. Fry, and I.G. Wright, "Managing steam-side oxidation and exfoliation in USC boiler tubes," *Advanced Materials and Processes*, 171, (1) pp. (2013).

21. A.S. Sabau, I.G. Wright, J.P. Shingledecker, and P.F. Tortorelli, "Managing oxide scale exfoliation In boilers with TP347h superheater tubes," *Proc. 7th International Conference on Advances in Materials Technology for Fossil Power Plants*, Waikoloa, Hawaii. EPRI 2014.
22. M. Shütze, M. Malessa, D. Renusch, P.F. Tortorelli, I.G. Wright, and R.B. Dooley, "Mechanical properties and adherence of oxide scales," *Materials Science Forum*, 522, 393-400 (2006).
23. S. C. Kung, "Guide to Grade 91 Use Temperature Limits Due to Steam Oxidation and Exfoliation," EPRI Report No. 3002011137, August 2017.